PAPER • OPEN ACCESS

The QUBIC instrument for CMB polarization measurements

View the article online for updates and enhancements.
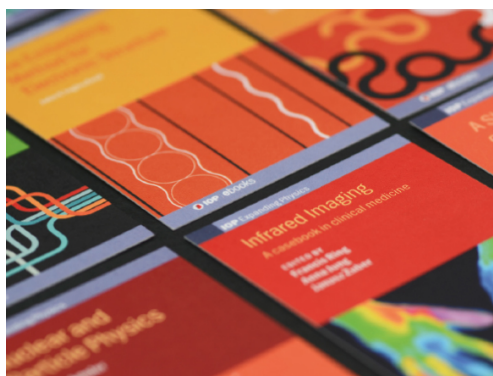
IOP ebooks™

Bringing together innovative digital publishing with leading authors from the global scientific community.

Start exploring the collection–download the first chapter of every title for free.

The QUBIC instrument for CMB polarization measurements

L Mele [1,2], **P Ade** [3], **J G Alberro** [4], **A Almela** [5], **G Amico** [1], **L H Arnaldi** [6], **D Auguste** [7], **J Aumont** [8], **S Azzoni** [9], **S Banfi** [10,11], **E S Battistelli** [1,2], **A Baù** [10,11], **B Bélier** [12], **D Bennett** [13], **L Bergé** [14], **J-Ph Bernard** [8], **M Bersanelli** [15], **M-A Bigot-Sazy** [16], **N Bleurvacq** [16], **J Bonaparte** [17], **J Bonis** [7], **A Bottani** [4], **E Bunn** [18], **D Burke** [13], **D Buzi** [1], **F Cavaliere** [15], **P Chanial** [16], **C Chapron** [16], **R Charlassier** [16], **F Columbro** [1,2], **A Coppolecchia** [1,2], **G D'Alessandro** [1,2], **P de Bernardis** [1,2], **G De Gasperis** [19], **M De Leo** [1], **M De Petris** [1,2], **S Dheilly** [16], **L Dumoulin** [14], **A Etchegoyen** [5], **A Fasciszewski** [17], **L P Ferreyro** [5], **D Fracchia** [5], **C Franceschet** [15], **M M Gamboa Lerena** [4], **K Ganga** [16], **B García** [5], **M E García Redondo** [5], **M Gaspard** [7], **D Gayer** [13], **M Gervasi** [10,11], **M Giard** [8], **V Gilles** [1], **Y Giraud-Heraud** [16], **M Gómez Berisso** [6], **M González** [6], **M Gradziel** [13], **L Grandsire** [16], **J -Ch Hamilton** [16], **D Harari** [6], **S Henrot-Versillé** [7], **D T Hoang** [16], **F Incardona** [15], **E Jules** [7], **J Kaplan** [16], **C Kristukat** [17,20], **L Lamagna** [1,2], **S Loucatos** [16], **T Louis** [7], **B Maffei** [21], **S Marnieros** [14], **W Marty** [8], **S Masi** [1,2], **A Mattei** [2], **A May** [9], **M McCulloch** [9], **S Melhuish** [9], **A Mennella** [15], **L Montier** [8], **L Mousset** [16], **L M Mundo** [4], **J A Murphy** [13], **J D Murphy** [13], **F Nati** [10,11], **E Olivieri** [14], **C Oriol** [14], **C O'Sullivan** [13], **A Paiella** [1,2], **F Pajot** [8], **A Passerini** [10,11], **H Pastoriza** [6], **A Pelosi** [2], **C Perbost** [16], **M Perciballi** [2], **F Pezzotta** [15], **F Piacentini** [1,2], **M Piat** [16], **L Piccirillo** [9], **G Pisano** [3], **M Platino** [5], **G Polenta** [22], **D Prêle** [16], **R Puddu** [23], **D Rambaud** [8], **P Ringegni** [4], **G E Romero** [24], **M Salatino** [25], **J M Salum** [5], **A Schillaci** [26], **C Scóccola** [4], **S Scully** [13], **S Spinelli** [10], **G Stankowiak** [16], **M Stolpovskiy** [16], **A Tartari** [27], **J-P Thermeau** [16], **P Timbie** [28], **M Tomasi** [15], **S Torchinsky** [16], **M Tristram** [7], **G Tucker** [29], **C Tucker** [3], **D Viganò** [15], **N Vittorio** [19], **F Voisin** [16], **F Wicek** [7], **M Zannoni** [10,11], **A Zullo** [2]

[1] Dipartimento di Fisica, Sapienza Università di Roma, piazzale Aldo Moro 5, 00185, Roma, Italy

[2] Istituto Nazionale di Fisica Nucleare Roma 1 Section, piazzale Aldo Moro 5, 00185, Roma, Italy

[3] School of Physics and Astronomy, Cardiff University, Cardiff CF10 3AT, UK

[4] Facultad de Ciencias Astronómicas y Geofísicas, Univ. Nacional de la Plata, La Plata B1900FWA, Argentina

[5] Instituto de Tecnologías en Detección y Astropartículas, Buenos Aires B1650, Argentina

[6] Ctr. Atómico Bariloche e Instituto Balseiro, CNEA, San Carlos de Bariloche R8402AGP, Argentina

[7] Laboratoire de l'Accélérateur Linéaire (CNRS-IN2P3), 91898 Orsay, France

[8] Institut de Recherche en Astrophysique et Planétologie (CNRS-INSU), 31028 Toulouse, France

[9] School of Physics & Astronomy, University of Manchester, Manchester M13 9PL, UK

[10] Department of Physics, Università di Milano Bicocca, 20126 Milano, Italy

[11] Istituto Nazionale di Fisica Nucleare Milano Bicocca section, 20126 Milano, Italy

[12] Centre de nanosciences et de nanotechnologies, 91120 Palaiseau, France

[13] Department of Experimental Physics, University of Ireland, Mariavilla, Maynooth 99MX+QH, Ireland

[14] Centre de Spectrométrie Nucléaire et de Spectrométrie de Masse (CNRS-IN2P3), 91405 Orsay, France

[15] Department of Physics, University of Milan, 20133 Milano, Italy

[16] Astroparticule et Cosmologie (CNRS-IN2P3), 75013 Paris, France

[17] Comisión Nacional De Energia Atómica,Salta A4400, Argentina

[18] Department of Physics, Richmond University, Richmond, VA 23173, USA

[19] Dipartimento di Fisica, Università di Roma Tor Vergata, 00133 Roma, Italy

[20]Escuela de Ciencia y Tecnología, Universidad Nacional de San Martín, San Martin 1650, Argentina

[21] Institut d'Astrophysique Spatiale (CNRS-INSU), 91405 Orsay, France

[22] Agenzia Spaziale Italiana, 00133 Rome, Italy

[23] Instituto de Astrofísica, Pontificia Universidad Católica de Chile, 4860 Santiago, Chile

[24] Instituto Argentino de Radioastronomía, Berazategui 1880, Argentina

[25] Kavli Institute for Particle Astrophysics and Cosmology, Stanford California 94305, USA

[26] California Institute of Technology, Pasadena CA 91125, California, USA

[27] Istituto Nazionale di Fisica Nucleare Pisa Section, 56127 Pisa, Italy

[28] Department of Physics, University of Wisconsin, Madison, WI 53706, USA

[29] Department of Physics, Brown University, Providence, RI 02912, USA

E-mail: `lorenzo.mele@roma1.infn.it`

Abstract. Measurements of cosmic microwave background (CMB) polarization may reveal the presence of a background of gravitational waves produced during cosmic inflation, providing thus a test of inflationary models. The Q&U Bolometric Interferometer for Cosmology (QUBIC) is an experiment designed to measure the CMB polarization. It is based on the novel concept of bolometric interferometry, which combines the sensitivity of bolometric detectors with the properties of beam synthesis and control of calibration offered by interferometers. To modulate and extract the input polarized signal of the CMB, QUBIC exploits Stokes polarimetry based on a rotating half-wave plate (HWP). In this work, we illustrate the design of the QUBIC instrument, focusing on the polarization modulation system, and we present preliminary results of beam calibrations and the performance of the HWP rotator at 300 K.

1. Introduction

A certain degree of linear polarization was imprinted in the cosmic microwave background (CMB) by Thomson scattering between electrons and radiation with a quadrupole anisotropy. At the time the CMB was released, one of the sources of anisotropies were tensor fluctuations, in the form of a stochastic background of gravitational waves eventually generated by cosmic inflation, which should have imprinted a characteristic polarization pattern, called B-mode [1]. The detection of CMB B-modes would be a smoking-gun evidence for cosmic inflation but to date a positive confirmation is still missing and only upper-limits have been set on their amplitude [2]. The expected signal is extremely weak, with an amplitude smaller than few nK not tightly constrained by theoretical predictions. Besides the intrinsic amplitude of the signal, measurements of the B-modes are plagued by polarized foregrounds, gravitational lensing and instrumental systematic effects [1]. The Q&U Bolometric Interferometer for Cosmology (QUBIC) is a ground-based experiment designed to measure B-modes, exploiting the novel concept of bolometric interferometry, which combines high sensitive bolometric detectors with the beam synthesis capabilities of interferometers. It has been demonstrated that bolometric interferometers can reach the same sensitivity as imagers with the same number of detectors [3]. In addition, bolometric interferomenters can exploit the so-called *self calibration* [3] to control and correct several systematic effects [4, 5]. For all these reasons we expect that QUBIC will face different systematic effects from those of the CMB imagers (see e.g. [6, 7] and references therein): this is an important asset, given the extremely low level of the target B-modes. Moreover, differently from other experiments from ground which allow observations at a few frequency bands because of contamination by the Earth's atmosphere, QUBIC allows the separation of the CMB signal from polarized foregrounds. Indeed, its spectral-imaging capabilities allow the extrapolation of the signal at several frequency sub-bands within the main channels, with a spectral resolution of $\Delta\nu/\nu \sim 0.05$ [8]. In this paper, we describe the QUBIC instrument in Sec. 2. The synthetic beam, together with the preliminary results on its calibration, are presented in Sec. 3. Finally, the polarization modulation system and its performance at 300 K are treated in Sec. 4.
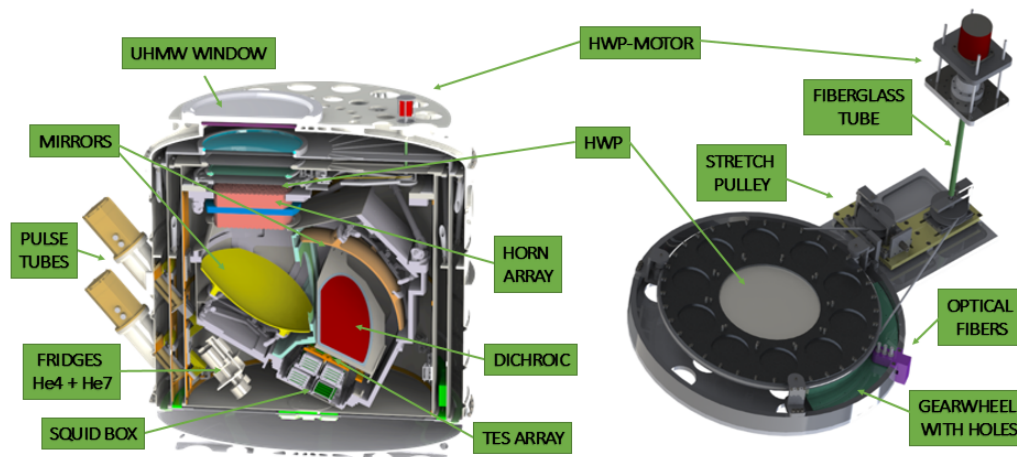
Figure 1: Schematic overview of the QUBIC instrument (left panel) and of the HWP rotator (right panel).

2. The QUBIC Instrument

Bolometric interferometry is the basic concept of the QUBIC instrument (schematized in Fig. 1), where the combination of an array of 400 back-to-back corrugated feedhorns [9] with a beam combiner produces interference fringes. The array of back-to-back horns consists of the following elements: 400 primary horns, which collect modulated radiation; an array of switches, consisting of a series of blades that act as shutters of circular waveguides at the end of each primary horn; an array of 400 secondary horns, which direct the light towards the beam combiner. The array of switches will be used in open configuration during the final observations. On the other hand, during the self calibration process, they allow the exclusion of single horn pairs. When excluding equivalent horn pairs, i.e. couples of horns at the same distance and with the same orientation in the array, the same fringe pattern should be produced on the focal planes in absence of systematic effects. This procedure, described in details in [3], provides thus an extremely powerful tool to highlight the effect of instrumental systematics. The photometric apparatus of QUBIC is completed by two orthogonal focal planes, each equipped with 1024 TES bolometers, with a noise equivalent power (NEP) of 10^{-17} W/$\sqrt{Hz}$ [10]. Two frequency bands are selected through a dichroic filter, which transmits radiation at 150 GHz and reflects back radiation at 220 GHz. To extract the polarization of the input light, a rotating half-wave plate (HWP) [11] followed by a linear polarizer is used to modulate the polarized component of the CMB. All the above elements are located inside a large cryostat where the light enters through a 45 cm diameter ultra high molecular weight (UHMW) window [12]. Two intermediate shells reduce radiative loads in the cryogenic components of the instrument and they are cooled down at 40 and 4 K with two double-stage pulse tubes. A single-stage ^{4}He fridge refrigerates the optics box at 1 K and an ^{4}He/^{3}He sorption fridge is used to refrigerate the focal planes at 300 mK [13].

3. Synthesized Beam

Interferometers have been widely used at mm wavelengths, where the signals from pairs of horn antennas (baselines), extracted from an array, get multiplied to measure a set of visibilities, which are related to the sky image via Fourier transform. QUBIC employs a Fizeau interferometer which adds the signals, instead of multiplying them, and which allows measurements in both visibility and image space simultaneously, selecting only a sub-set of the modes from the sky through the horn array. Each baseline selects a specific Fourier mode from the sky, and all possible configurations of horn pairs produce fringe patterns that sum up directly on the focal planes, where a synthetic image of the sky is produced. The synthetic image is the convolution between the signal from the sky, X, and and the synthesized beam of each detector of the
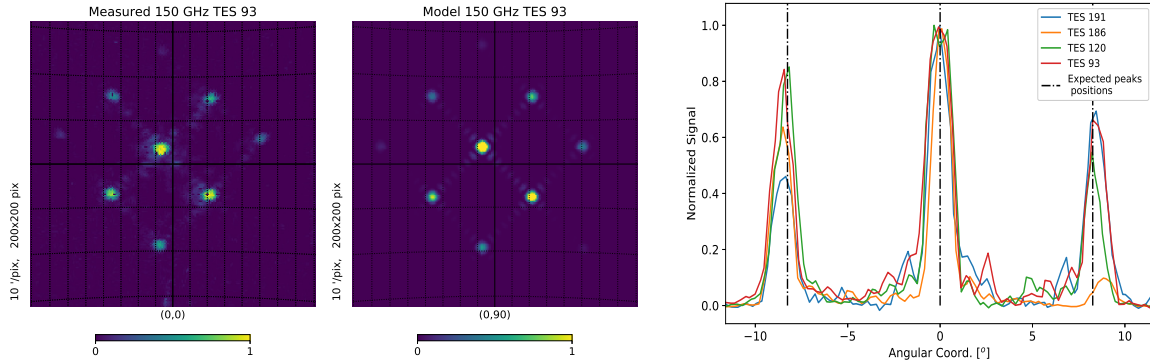
Figure 2: Left: Measured synthesized beam of the TES bolometer number 93 in the 150 GHz array of the TD, compared with the theoretical forecast without aberrations. Right: 45° cut of the synthetic beams of the TES bolometers number 93, 120, 186 and 191 at 150 GHz, normalized at their maximum.

instrument, B^p_{synth}, so that the expected signal registered by the detector p is:

$$S_X(p) = \int X(\hat{n}) B^p_{synth}(\hat{n}) d\hat{n} \qquad (1)$$

where $\hat{n}$ defines the direction of the line of sight. The signal from the sky is characterized by the three Stokes parameters: the intensity I and linear polarizations Q and U. This fact implies that QUBIC data can be analyzed similarly to data taken from a traditional imager, provided that we know the shape of the synthesized beam for each detector. The pattern of the synthesized beam of the central detector at 150 GHz is composed of a central primary peak, with 0.54^o full width at half maximum (FWHM), and secondary peaks spaced by 8.5^o from the main peak. The relative separation between the primary and the secondary peaks of the beam of a specific detector grows linearly with the frequency [8]. At the same time, the relative separation at a given frequency remains unchanged for different detectors on the focal plane. We show in the left panel of Fig. 2 the measured synthetic beam for the detector number 93 in the Technological Demonstrator (TD) of the QUBIC instrument as an example, compared to the theoretical signal neglecting the effect of aberrations. The QUBIC-TD is currently being calibrated in the Astroparticle and Cosmology Laboratory (APC), in Paris, and it consists of a reduced array of 64 back-to-back feedhorns and one-quarter of the 150 GHz TES array. The synthesized beam pattern is consistent with our model in terms of peaks positions. This is better shown in the right panel of Fig. 2, where 45° cuts of normalized beams of the TESes number 93, 120, 186 and 191 show that the peaks relative position is in agreement with the expectations at 150 GHz, with secondary peaks separated $\sim 8^o$ from the primary peak. The relative separation of the peaks is the same for the four detectors as expected at a given frequency. The shape of the pattern will be validated only when saturation issues will be solved and the self calibration approach will be possibly applied.

4. Half-Wave Plate Rotator

Stokes Polarimetry is a well-known technique to recover the linear polarization of the incoming radiation [14]. A Stokes polarimeter is basically a rotating HWP followed by a linear polarizer. The optical power reaching the detector p on the focal plane for a given frequency ν, and for a specific orientation of the HWP, θ, is:

$$I(p, \nu, \theta) = \frac{1}{2}[S_I(p, \nu) + S_Q(p, \nu) \cdot \cos(4\theta) + S_U(p, \nu) \cdot \sin(4\theta)] \qquad (2)$$

where S_I, S_Q and S_U are the Stokes components from the sky convolved with the synthesized beam of the detector p. The HWP rotator, schematized in the right panel of Fig. 1, allows one to modulate the
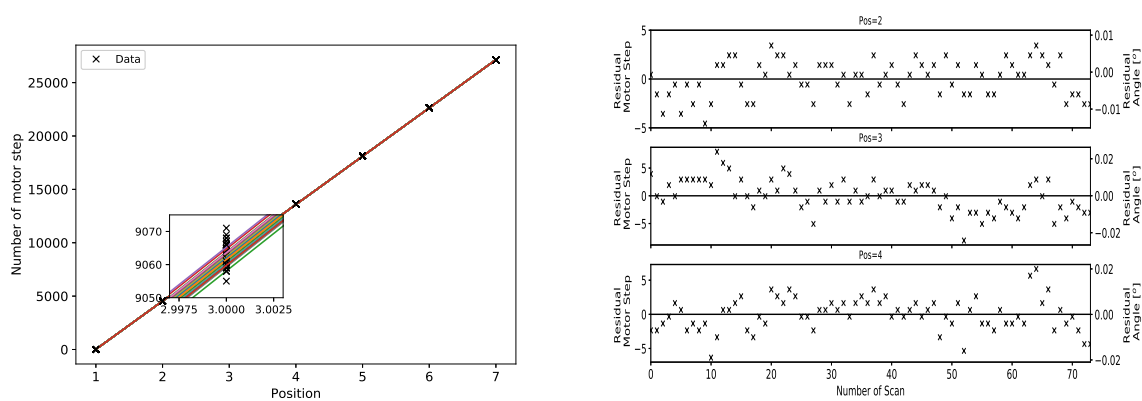
Figure 3: Left: number of motor steps with respect to rotator positions, with corresponding linear fits, acquired in 75 clockwise scans performed at 300 K. Right: residual in terms of motor steps and rotation angles for the measurements at the 2nd, 3rd and 4th positions as representative cases.

polarized component of the input radiation by changing the orientation of the plate, so that the Stokes parameters can be extracted according to the Eq. 2. The rotation is generated by an external stepper motor and it is transmitted through a fiberglass tube and a system of pulleys to the rotator, placed on the top of the 4 K stage. The fiberglass tube limits heat flows from the outer shell at 300 K to the 4 K shield. A steel cord is wrapped around the pulleys and the rotator primary ring, where the HWP is fixed, and one of the pulleys is loaded with a spring to balance differential contraction of aluminum parts during the cooldown. The rotator is a device which can move to 7 positions, with steps of 15°, covering 90° of rotation. The readout system is an optical encoder, where three couples of optical fibers, which transmit infrared light generated by an oscillator, face each other. A gearwheel with 7 series of holes, which define the positions, rotates together with the primary ring, sliding between the two series of optical fibers. When the optical fibers and the holes are aligned, the signal can travel through the fibers and it is thus detected by photodiodes and lock-in amplified using an AD630-based custom synchronous demodulator [15]. The signals from the lock-in amplifiers are processed by a custom software running on a Raspberry Pi3 (RbPi), which recovers the HWP orientation with $< 0.1^o$ accuracy. The RbPi also controls the stepper motor, rotating the HWP according to the scan strategy of the sky.

4.1. 300 K Test:
The HWP rotator has been successfully tested at room temperature on an optical bench, with 75 scans performed for each direction of rotation. Data are in the form of number of motor steps with respect to the rotator position and they are acquired by the RbPi when the position is actually reached. In the left panel of Fig. 3 we show all the scans for the clockwise rotation together with the corresponding linear fit. In the same figure a zoom around the 3rd position is reported. Keeping in mind that a single motor step corresponds to a rotation of 0.003^o, this figure highlights great reproducibility, since the curves overlap within a few motor steps. The same result is better shown in the right panel of Fig. 3, which shows that the residuals of the motor steps needed to reach the positions 2, 3 and 4 in 75 scans are within ~ 10 motor steps. We report the residuals for some representative cases; the same results are achieved for all positions and for the counterclockwise rotation.

4.2. Further Analysis
Considering both directions of rotation, we can calibrate our instrument including information about the size of single positions defined by the gearwheel. Since the count of motor steps is acquired by the RbPi when a position is read by the readout system, the acquisition occurs at the left edge of the position for
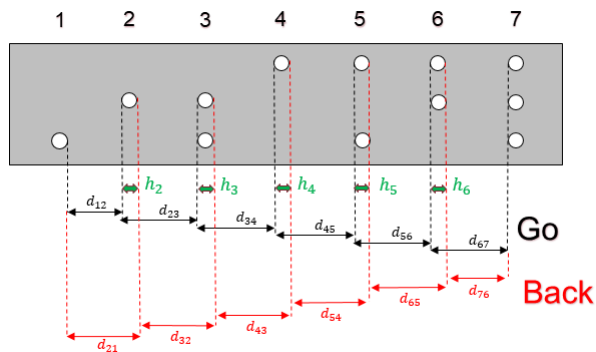
Figure 4: Scheme of the gearwheel equipped with 7 series of holes, defining the rotator positions. Combining data from both directions of rotations, the size of intermediate positions can be extracted.

h_i	motor steps	degrees
h_2	87.7 ± 0.5	0.291 ± 0.002
h_3	64.9 ± 0.5	0.216 ± 0.002
h_4	115.5 ± 0.7	0.383 ± 0.002
h_5	66.8 ± 0.8	0.222 ± 0.003
h_6	89.9 ± 0.6	0.299 ± 0.002

Table 1: Mean values and errors on the mean for the size of intermediate positions extracted combining data at 300 K from both directions of rotation.

the clockwise rotation and at the right edge for the counterclockwise rotation. This is illustrated in Fig. 4 as a schematic of the gearwheel with motor steps counts d_{xy} from position x to position y. Combining counts of motor steps from both directions of rotation, we are able to recover how many motor steps are necessary to cross the single position, labelled as h_i in Fig. 4. Since the rotator can move between the first and the last position, this analysis can only be performed for intermediate positions. In Tab. 1 we report the size of the h_i terms as motor steps and degrees of rotation. This result shows that, with a suitable calibration of the motor steps, we are allowed to move the HWP at specific positions with high precision, also at non-nominal positions (not defined by the gearwheel).

5. Conclusions

QUBIC is designed to face all the aspects of the B-mode research. Specifically, the self calibration procedure promises the required control over many systematic effects, which are extremely important for current and future CMB experiments. The first measurement of the synthetic beam represents a step forward to the interferometric capabilities of QUBIC, which will reach full potential after the final calibration of the QUBIC-TD, scheduled for december 2019. The HWP rotator has been validated at 300 K and its performance at 4 K is being tested. After the calibrations, the QUBIC-TD will be deployed to the observational site in Alto Chorillos, 4560 m above sea level, in Argentina, where its scientific potential will be tested. The final instrument installation is scheduled for 2020.

References

[1] Kamionkowski M and Kovetz E D 2016 *Annu. Rev. Astron. Astrophys.* **54** 227-269
[2] BICEP2/Keck and Planck Collaborations 2015 *Phys. Rev. Lett.* **114** 101301
[3] Bigot-Sazy M-A, Charlassier R, Hamilton J-Ch ,Kaplan J and Zahariade G 2013 *A.&A.* **550**
[4] The BICEP2 Collaboration 2015 *ApJ* **814** 110
[5] D'Alessandro G, Mele L, Columbro F, Piacentini F, Pagano L, de Bernardis P, Masi S 2019 *A.&A.* **627**
[6] Henderson S W , Allison R, Austermann J *et al.* 2016 *J. Low. Temp. Phys.* **184** 772-779
[7] Anderson A J, Ade P A R , Ahmed Z *et al.* 2018 *J. Low. Temp. Phys.* **193** 1057-65
[8] Mennella A *et al.* 2019 *Universe* **5** 42
[9] Maffei B *et al. Proc. of SPIE* 2014 Montréal vol 9153 ed Holland W S and Zmuidzinas J
[10] Salatino M *et al. Proc. of SPIE* 2018 Austin vol 10708 ed Zmuidzinas J and Gao J-R
[11] Pisano G *et al. Proc. of SPIE* 2014 Montréal vol 9153 ed Holland W S and Zmuidzinas J
[12] D'Alessandro G *et al.* 2018 *Infrared Phys. Technol.* **90** 59-65
[13] May A *et al. Proc. of SPIE* 2018 Austin vol 10708 ed Zmuidzinas J and Gao J-R
[14] Wu J H P *et al.* 2007 *Astrophys. J.* **665** 42
[15] Meade M L 1983 *Lock-in Amplifiers: Principles and Applications* (IEE Electrical Measurement Series vol 1)